41st Aerospace Sciences Meeting and Exhibit
6-9 January 2003, Reno, Nevada

AIAA 2003-0546

WIND VALIDATION CASES: COMPUTATIONAL STUDY OF THERMALLY-PERFECT GASES

T. DalBello*
Institute for Computational Mechanics in Propulsion (ICOMP)
NASA Glenn Research Center, Cleveland, OH 44135

Abstract

The ability of the WIND Navier-Stokes code to predict the physics of multi-species gases is investigated in support of future high-speed, high-temperature propulsion applications relevant to NASA's Space Transportation efforts. Three benchmark cases are investigated to evaluate the capability of the WIND chemistry model to accurately predict the aerodynamics of multi-species chemically non-reacting (frozen) gases. Case 1 represents turbulent mixing of sonic hydrogen and supersonic vitiated air. Case 2 consists of heated and unheated round supersonic jet exiting to ambient. Case 3 represents 2-D flow through a converging-diverging Mach 2 nozzle. For Case 1, the WIND results agree fairly well with experimental results and that significant mixing occurs downstream of the hydrogen injection point. For Case 2, the results show that the Wilke and Sutherland viscosity laws gave similar results, and the available SST turbulence model does not predict round supersonic nozzle flows accurately. For Case 3, results show that experimental, frozen, and 1-D gas results agree fairly well, and that frozen, homogeneous, multi-species gas calculations can be approximated by running in perfect gas mode while specifying the mixture gas constant and Ratio of Specific Heats.

* Senior Research Associate, Department of Mechanical Engineering, University of Toledo, Toledo, Ohio. Member AIAA.Email: *teryn.w.dalbello@grc.nasa.gov.*
This document is intended to be viewed in color. v2.

1. Introduction

THIS PAPER presents the results of benchmark validation studies used to evaluate the capability of WIND[1] to predict the physics of a mixture of gases in internal geometries in support of future high-speed, high-temperature propulsion applications relevant to NASA's Space Transportation efforts. Accurate prediction of the aerodynamics requires correct modeling of the macroscopic chemistry effects, which includes the production and consumption of species (combustion), thermal and mass diffusion and other species interactions. Development, verification, and validation of the NPARC Alliance WIND solver has been proceeding over the past several years. Recent work has included improving the thermally-perfect gas (frozen), equilibrium air, and non-equilibrium air models. This paper focuses on the validation of thermally-perfect gas models in which no chemical reactions are taking place.

The evaluation cases used here to benchmark recent changes to WIND, collected from the National Combustion Code (NCC)[2] validation archive, consist of calculations on chemically non-reacting (frozen) mixtures of gases, intended to study mixing and, ultimately, combustion in a simplified engine nozzle or combustor. Frozen gases obey the perfect gas law but have locally varying specific heats. The internal flow problems shown in the archive can give indications about deficiencies inherit to the turbulence models, chemistry models, reaction rate and thermodynamic coefficients, and main flow equations. For this paper, experimental and numerical results for three cases are compared to calculations using WIND version 5.

The first case represents mixing of sonic hydrogen and a supersonic vitiated airstream[3]. The second case consists of calculations on a heated and unheated round supersonic jet exiting to ambient[4]. Finally, the

third case represents flow through a 2-D converging-diverging Mach 2 nozzle[5].

2. Numerical Model

Calculations were conducted with WIND v5.0 *alpha*, a general purpose 3-D Computational Fluid Dynamics (CFD) code which solves the turbulent, time-dependent, Reynolds-Averaged Navier-Stokes equations, in addition to the equations which govern equilibrium air, non-equilibrium air and frozen gas chemistry. For the calculations presented here, the solver was configured to run with the following specifications:

- Two-dimensional or axisymmetric, steady-state
- Frozen chemistry and perfect gas models
- Sutherland and Wilke viscosity laws
- Node-centered finite-volume approach
- Second order Roe upwind scheme
- Two-equation Menter SST (Shear Stress Transport) turbulence model

WIND was configured to run in multi-processor mode on an SGI Origin 2000. As mentioned, Sutherland[6] and Wilke[7] laws are both used to compute laminar viscosity for the three cases studied. For frozen and perfect gas runs, the local static temperature and associated reference values (for air) are used to compute viscosity in Sutherland's law:

$$\mu_{lam} = \mu_o \left(\frac{T}{T_o} \right)^{\frac{3}{2}} \left(\frac{T_o + S}{T + S} \right)$$

where T is the local static temperature, and μ_O, S and T_O are reference values for air.

Wilke's law, an extension of the Sutherland-type equation to multi-component systems obtained on the basis of the kinetic theory and several simplifying assumptions, is used in WIND to compute the laminar viscosity for multi-species gases:

$$\mu_{lam} = \sum_{i=1}^{N} \frac{X_i \cdot \mu_i}{\sum_{j=1}^{N} X_j \cdot \phi_{i,j}}$$

where

$$\phi_{i,j} = \frac{1}{\sqrt{8}} \left(1 + \frac{M_i}{M_j} \right)^{-1/2} \left[1 + \sqrt{\frac{\mu_i}{\mu_j}} \left(\frac{M_j}{M_i} \right)^{1/4} \right]^2$$

where $\phi_{i,j}$ is the mixing coefficient, X is the species mole fraction, M is the species molecular weight, and μ is the species laminar viscosity computed with Sutherland's law. Because the species viscosity in Wilke's law is initially computed with Sutherland's law, the mixture viscosity is still a function of temperature, but is potentially more accurate in that it is calculated using information about the molecular composition of the mixture. The mixture thermal conductivity is also calculated using Wilke's law but with different reference values.

Thermodynamic, transport and finite rate coefficients used by the chemistry equations are not hard-coded into WIND, allowing the user freedom to specify different chemical mechanisms. Changes to these coefficients can have significant effects on the results, as observed in some undocumented trials. For frozen cases, only the thermodynamic and transport coefficients listed in the chemistry input files are used by the chemistry equations (the reaction rates are zero for frozen reactions). Holding total temperature and pressure fixed at the inflow plane when using chemistry is currently not implemented in WIND. As a result, unless otherwise specified, all inflow values are specified as static values in this report. For Case 2, these values were adjusted slightly so that the final total temperature and pressure matched the conditions of the experiment.

Two-dimensional, structured, computational grids were generated for all cases using Pointwise, Inc's GRIDGEN[8] software. Average y+ values on the viscous walls were specified to be approximately 1.

The convergence criterion consisted of monitoring the species mass fractions at the computational domain exit for changes with iteration, at least two orders of magnitude reduction of the L2 Norm residual, and mass flow conservation.

3. Description of Cases and Results

Case 1: Mixing

Case 1 represents non-combusting turbulent mixing of two supersonic streams whose chemical composition is fixed (frozen). It consists of a hot, high-speed vitiated mixture entering above and parallel to a sonic stream of pure hydrogen. Both streams enter into the 3.66 inch high by 14 inch long combustor. The hydrogen injection height at the injection step is 0.157 inches from the bottom wall, followed by a lip region of 0.03 inches, and 3.5 inches of freestream.

This case was modeled using a 2-D, 5-zone grid (see Figure 1) with 363 points streamwise and 159 points vertically representing the mixing (test) section of the experiment, and a 50 by 81 zone upstream to develop boundary layers in the vitiated stream. The lower viscous wall of the mixing section is sloped to account for thickening of the boundary layer. Grid points were clustered along the lower viscous wall to resolve the turbulent boundary layer and in the shear layer between the two streams.

The conditions for Case 1 are shown in Table 1.

The freestream flow entering the mixing section represents vitiated air, whose mass fractions are 0.233 H_2O, 0.001 H_2, and 0.766 N_2. A 7-species, 8-reaction chemistry model is used to capture mixing and diffusion of species specified in the chemistry file *h2air-7sp-std-15k.chm*. The frozen BC was used for the freestream inflow, arbitrary inflow frozen BC for the hydrogen stream, the lower wall is adiabatic and no-slip, and the static pressure is extrapolated at the exit.

Table 1: Case 1 Flow Conditions

	Freestream	Hydrogen Stream
Mach No.	2.44	1.0
Temperature	2070 R (1150K)	540 R (300K)
Pressure	14.7 psi (101 kPa)	14.7 psi (101 kPa)
Turb. model	SST	SST
Viscosity Law	Wilke	Wilke
Species	H_2, H_2O, N_2	H_2
Wall BC	adiabatic	adiabatic

A grid dependence study was conducted on Case 1 to assess the effect of the computational grids on the solution accuracy. An exit profile of H_2O mass fractions is shown in Figure 2 for different grid sizes, giving an indication that the solution is not changing much with successive grid levels. The lowest values of H_2O occur to the left of the plot near the wall, where the sensitivity of the different grid sizes is most apparent. A grid size of 363x159 was used for the calculations presented here.

Case 1 results are shown in Figures 4 through 10, and are compared with numerical and experimental results found in Reference 3. Figures 5 through 7 give a qualitative overview of the boundary layer and shear layer development and thicknesses, highlighted by the H_2O, Mach number and turbulent viscosity profiles. The two inflow streams, along with the inflow boundary layer and lip region, drive the mixing in this problem, and contribute to the vertical diffusion of both layers at the exit of the combustor. Species mixing is illustrated in Figure 4, which shows H_2, N_2, and H_2O axial contours through the duct in two different directions. The solid lines show cuts parallel with the wall, and the dashed lines show cuts straight across the duct (not sloping, but in the true *x*-direction). As indicated in Figure 3, the cuts start at the hydrogen inflow plane 0.0785 inches off the bottom wall and traverse downstream. Turbulent mixing and movement of hydrogen away from the wall and replacement with H_2O and N_2 progressively further down the duct can be seen. Significant mixing starts to occur at about five inches downstream of the hydrogen injection point (plotting along the wall). This turbulent mixing process is critical to existence of combustion, and the specific ignition location (assuming it was combusting). Mass fractions of species at the entrance and exit of mixing section are conserved down to seven decimal places. The hydrogen stream enters the mixing section slightly underexpanded in the final solution (although the initial pressures between the two streams were set equal), and expansion waves form off the lip, further increasing the mixing between the two streams (see Figure 3). Figures 8, 9, and 10 show species mass fractions for nitrogen, hydrogen, and water at the duct exit for the experimental, NASTD, and WIND results. The *x*-axis of these plots goes from the top wall to the bottom wall (left hand side of the plot represents the boundary layer region on the lower viscous wall). The original NASTD[10] (precursor to WIND) results were computed using the PDT algebraic turbulence model. The WIND results are computed (using the SST model); both the Chien k-ε and PDT algebraic models failed to develop a turbulent viscosity profile in the mixing layer. Nevertheless, the WIND results (using the SST model) compare fairly well with the experiment, although the experimental data points do not extend into the boundary layer. Differences between the WIND and NASTD results are most apparent in the boundary layer. In Figure 9, a lower mass fraction of hydrogen at the wall was predicted by WIND compared with NASTD.

Case 2: Supersonic Jet Flow

Case 2 represents subsonic air flowing through an axisymmetric converging-diverging nozzle and accelerating supersonically, representing flow through a generic fighter jet engine nozzle exiting into the ambient. This case consists of a homogeneous oxygen/nitrogen mixture (air) flowing through the nozzle. Two different inflow temperatures were tested as part of Case 2, representing cold (104^o F, Subcase 2A) air, and hot (1550^o F, Subcase 2B) air accelerated supersonically, and exiting into ambient air (see Figure 11). For these two temperatures, both frozen chemistry and perfect gas runs were completed, for a total of four runs. This case was run in axisymmetric mode. The inflow conditions for the nozzle are shown in Table 2. The ambient region has an inflow Mach number of 0.01.

The grid for Case 2 (Figure 12) consists of three zones. The first represents the internal nozzle region and is 121 x 81 points. Zone 2 is the inflow for the ambient region, consisting of 41 axial and 34 vertical

points. The ambient exhaust region represented as zone 3 consists of 121 axial and 121 vertical points, and goes 25 nozzle diameters downstream (the nozzle diameter is 0.3 ft). The lower inviscid wall is the nozzle centerline. The grid sizing for Case 2 was determined to be sufficient as indicated in Reference 11.

The frozen runs have an inflow consisting of air, represented as 0.23 mass fraction oxygen and 0.77 mass fraction nitrogen (to compare directly with the perfect gas case). The laminar viscosity was computed with both Sutherland and Wilke laws. The default 7-species, 8-reaction chemistry mechanism was used, specified by the chemistry file *h2air-7sp-std-15k.chm*. The arbitrary inflow BC was used at the nozzle and plenum inflows, the internal nozzle upper adiabatic wall is viscous, and the other walls are inviscid (to represent the nozzle centerline). The Menter SST model was used to compute the eddy viscosity. For all Case 2 runs (frozen or perfect gas), temperature and pressure were specified in the WIND input file as static values. For Subcase 2A, the total temperature values listed in Table 1 were lowered 8 degrees in order to force matching of total temperature at the nozzle entrance with the experiment.

Table 2: Case 2 Flow Conditions

	Internal Nozzle Subcase2A: (104 F)	Internal Nozzle Subcase2B: (1550 F)
Mach No.	0.2	0.2
Total Temperature	104 F (564R)	1550 F (2010R)
Total Pressure	115.0 psi (793 kPa)	115.0 psi (793 kPa)
Turb. Model	SST	SST
Viscosity Law	Sutherland	Sutherland & Wilke
Species	oxygen, nitrogen (air)	oxygen, nitrogen (air)
Chemistry model	frozen & perfect gas	frozen & perfect gas
Wall BC	adiabatic	adiabatic

Case 2 results are shown in Figures 13 through 22 for Subcases 2A and 2B, both run with frozen chemistry and as a perfect gas. Figures 13 through 16 show contours of various flow properties for Subcase 2B. These give a qualitative view of how the flow expands into the exhaust region. Figures 15 and 16 show turbulent viscosity contours (normalized by freestream laminar viscosity) in the *x-y* plane which can be compared directly to examine the effects of the Sutherland and Wilke viscosity models. Similarly, radial profiles of the turbulent viscosity (normalized by the freestream laminar viscosity) at zone 3 exit are shown in Figure 17. It can be seen that Sutherland has a more pronounced effect in the subsonic portion of the flow away from the nozzle centerline. Close to the nozzle centerline, the two models give very similar results. Figures 18 and 19 show profiles of Mach number at the nozzle centerline starting at the exit of the nozzle and going about 25 nozzle diameters downstream for both subcases. This gives an indication of how the high-speed nozzle flow mixes into the very low Mach number ambient. The results shown here (and in Reference 11) indicate that the SST model, as well as the Chien k-ε model used in WIND, overpredict the mixing rates of supersonic jets. This can be seen from Figures 18 through 22 showing that Mach number, static and total temperature are not predicted correctly especially far away from the nozzle potential core. A total temperature plot for Subcase 2A is not shown because no experimental data was available. The frozen solution in Figure 20 shows a higher total temperature value (about 50 degrees) at the nozzle exit compared with the experiment, even though the total temperature and pressure values at the nozzle inflow held at the correct values. This is probably due to a postprocessing issue introduced when computing stagnation temperature (for a mixture of gases) from the solution file. The stagnation temperature is computed from Cp and static temperature, and Cp values used may be incorrect because they are not computed using the thermodynamic curve fit coefficients during postprocessing. Nevertheless, Case 2 results show that the frozen and perfect gas calculations are giving similar results for Subcase 2B (hot), but static and total temperature profiles for the Subcase 2A (cold) differ considerably.

Significant CPU time differences were seen when employing the chemistry equations. Subcase 2B (perfect gas) took 66.85 microseconds per node iteration; the frozen case took just over nine times more CPU time at 610 microseconds per node iteration. Use of the Wilke viscosity model boosted the CPU time from 610 to 710 microseconds per node iteration.

Case 3: Convergent-Divergent Nozzle

Case 3 represents subsonic, vitiated air exiting a combustor and accelerating supersonically through a Mach 2 convergent-divergent nozzle. This case was run 2-D. The frozen homogeneous mixture and perfect gas results are compared to experiment and 1-D analysis. One frozen calculation (Subcase 3A) and two perfect gas calculations (Subcases 3B and 3C) were completed. Flow conditions can be seen in Table 3. For the frozen case, mass fractions of the vitiated air were set to 0.233 for O_2, 0.226 H_2O, and 0.544 N_2. The ratio of the turbulent viscosity to the laminar viscosity was set to 0.01 at the inflow to match conditions used in the CFD analysis of the reference paper. Two perfect gas Subcases were completed: Subcase 3C with γ (ratio of spe-

cific heats) set to 1.4 and the gas constant set to 1716 ft^2/sec^2-R (287 m^2/s^2-K); Subcase 3B with γ set to 1.256 and the gas constant set to 1946 ft^2/sec^2-R (326 m^2/s^2-K), approximating the thermodynamic properties of the mixture in the frozen case. The γ=1.256 value used in Subcase 3B and in the 1-D analysis is the value that falls out from the solution of Subcase 3A in the core flow at the inflow plane of the nozzle. The arbitrary inflow BC was used for the inflow, viscous walls were set at 900R (500K), and the backpressure was forced at 14.7 psi. The Menter SST model was used to compute the turbulent viscosity, and Sutherland's law was used to compute the laminar viscosity for all subcases.

Table 3: Case 3 Flow Conditions

	Subcase3A	Subcase3B	Subcase3C
Mach No.	0.14	0.14	0.14
Temperature	3489 R (1940 K)	3489 R (1940 K)	3489 R (1940 K)
Pressure	111.5 psi (769 kPa)	111.5 psi (769 kPa)	111.5 psi (769 kPa)
Turb. Model	SST	SST	SST
Viscosity Law	Sutherland	Sutherland	Sutherland
Species	O_2, H_2O, N_2	air	air
Chem. Model	frozen	perfect gas	perfect gas
Ratio of Specific Heats	f(T)	1.256	1.400
R (local gas constant)	f(species)	1946 ft^2/sec^2-R	1716 ft^2/sec^2-R
Wall BC	isothermal	isothermal	isothermal

The 2-D grid for Case 3 (Figure 23) consists of one zone with 197 points axially (distributed equally) and 257 points vertically. Three grid levels were used to determine grid independence, and H_2O mass fractions at the exit plane are compared in Figure 24 for the three sizes. The fine grid (197x257) was used for calculations in this paper.

Case 3 results are shown in Figures 25 through 32. Three subcases were completed as part of Case 3: frozen chemistry Subcase 3A, perfect gas Subcase 3B (γ=1.256, R=1946 ft^2/sec^2-R), and perfect gas Subcase 3C (γ=1.4, R=1716 ft^2/sec^2-R). Figures 25 through 27 show the acceleration of gas through the nozzle constriction to supersonic speeds and subsequent changes in flow properties. Results from the three subcases are compared in Figures 28 through 32 to see the effects of the different chemistry models on the homogeneous mixture. In addition, 1-D analysis using area-Mach number relation and isentropic relations along the centerline of the duct is compared also. As seen in Figure 28, the frozen subcase and perfect gas subcase (γ=1.256) are close to the Pitot rake data and corresponding numerical results from the CFD code *VULCAN*[5,12]. Subcase 3C slightly overpredicts the Pitot pressure distribution compared with the experimental data. The 1-D Pitot pressure value for γ=1.256 is close to average values found from CFD and experiment in the core region of the flow. The 1-D Pitot pressure value for γ=1.4 shows a lower than expected pressure compared with the analogous WIND result (which slightly overpredicts the data). Figure 28 shows that approximating the frozen chemistry with constant values of γ and R is a very good approximation for problems involving homogenous mixture of species. This statement may be limited to cases with exit Mach numbers in the range of 2, and may not be valid for higher Mach number problems. The Pitot pressure is normalized by the total pressure in the heater of 7.62 atm (112 psi). Furthermore, plots of static pressure, temperature, Mach and *u*-velocity along the duct centerline shown in Figures 29 through 32 give some indication of the effects of the chemistry model. The WIND results are compared with values computed from the 1-D analysis using both γ=1.4 and 1.256. The agreement was fairly good, highlighted by the static temperature profile in Figure 29. Overall, the WIND perfect gas calculations with γ=1.4 show the most notable differences from the frozen results especially towards the exit of the nozzle. Lower initial turbulence levels (or a laminar run) tend to lower the pressure at the exit (less overall total pressure losses). CPU time was about 350 microseconds per node iteration for the frozen case, and 260 microseconds per node iteration for the perfect gas case.

4. Conclusions

Three different cases were the subject of CFD validations examining the frozen chemistry capability in WIND in support of future high-speed, high-temperature propulsion applications. The frozen calculations can be considered the building block for the more physically intensive and computationally demanding combustion cases. It has been shown that the frozen chemistry model gives fairly good comparison for the mixing problem (Case 1). The grid refinement study for Case 1 indicates that the 363 x 159 grid was sufficient to capture the mixing effects. As shown in the results for Case 2, the Wilke and Sutherland viscosity laws gave similar results, and the available turbulence models fail to pre-

dict supersonic nozzle flows correctly. Some slight differences between perfect gas and chemistry are seen between the static and stagnation temperature plots. Fairly good agreement was seen between experimental, numerical and 1-D analysis for Case 3. Although the flow solution for Case 3 tends to be one-dimensional, the grid refinement study indicates that the 197 x 257 grid was sufficient to capture the 2-D effects near the nozzle wall. The results for Case 3 indicate that multi-species gas calculations for problems involving homogeneous mixtures can be approximated by running in perfect gas mode while specifying the appropriate mixture gas constant and Ratio of Specific Heats. This conclusion may not be valid for high Mach number problems. Future studies could include the Chien k-ε and Spalart-Allmaras models and their effects, a possible analysis of mixing problems like Case 1 involving greater temperature and velocity differences between the primary and secondary streams, a jet in a crossflow (where the secondary flow is injected normal to the primary flow), as well as expansion of these problems to three dimensions.

5. Acknowledgements

This work is funded by NASA Grant/Cooperative Agreement number NCC3-922. Help from the following individuals made this work possible: Nick Georgiadis, John Slater, John Wolter, Dennis Yoder, Jim DeBonis, Rickey Shyne, Dennis Lankford, and Chris Nelson.

References

1) *The WIND User's Guide Version 5*, User Manual, The NPARC Alliance, July 7 2000, Cleveland, OH. http://www.grc.nasa.gov/WWW/winddocs index.html

2) Ebrahimi, H.B., Ryder R.C., Brankovic A., & Liu N.S., "A Measurement Archive for Validation for the National Combustion Code," AIAA Paper 2001-0811, January 2001.

3) Burrows, M.C., & Kurkov, A.P., "Analytical and Experimental Study of Supersonic Combustion of Hydrogen in a Vitiated Airstream," NASA-TM-X-2828, September 1973.

4) Seiner, J.M., Ponton, M.K., Jansen, B.J. & Lagen, N.T., "The Effects of Temperature on Supersonic Jet Noise Emission," DGLR/AIAA 14th Aeroacoustics Conference, Aachen, Germany, AIAA Paper 92-02-046, May 1992.

5) Springer, R.R., Cutler, A.D., Diskin, G.S., & Smith, M.W., "Conventional/Laser Diagnostics to Assess Flow Quality in a Combustion-Heated Facility," AIAA Paper 99-2170, June 1999.

6) White, F.M., *Viscous Fluid Flow*, McGraw-Hill, Inc., New York, NY, 1974.

7) Wilke, C.R., "A Viscous Equation for Gas Mixtures," *Journal of Chemical Physics*, Vol. 18, pp. 517-519, 1950.

8) *GRIDGEN Version 13*, User Manual, Pointwise, Inc. 1998, Bedford, Texas.

9) Menter, F.R., "Two-Equation Eddy-Viscosity Turbulence Models for Engineering Applications," *AIAA Journal*, Vol 32, No.8, 1994, pp. 1598-1605.

10) Mani, M., Bush, R.H., & Vogel, P.G., "Implicit Equilibrium and Finite-Rate Chemistry Models For High Speed Flow Applications," AIAA Paper 91-3299-CP, January 1991.

11) Dembowski, M.A., & Georgiadis, N.J., "An Evaluation of Parameters Influencing Jet Mixing Using the WIND Navier-Stokes Code," NASA/TM-2002-211727, August 2002.

12) White, J.A., & Morrison, J.H., "A Pseudo-Temporal Multi-Grid Relaxation Scheme for Solving the Parabolized Navier-Stokes Equations," AIAA Paper 99-3360, June 1999.

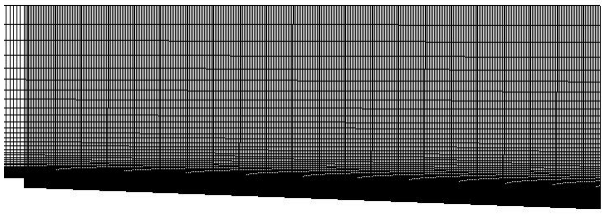

Figure 1: 363x159 grid for mixing section of Case 1.

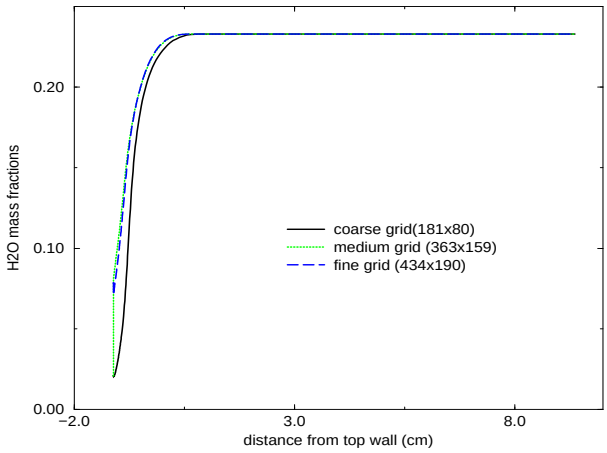

Figure 2: Case 1, H_2O mass fractions at mixing section exit plane, revealing the grid sensitivity of the solution.

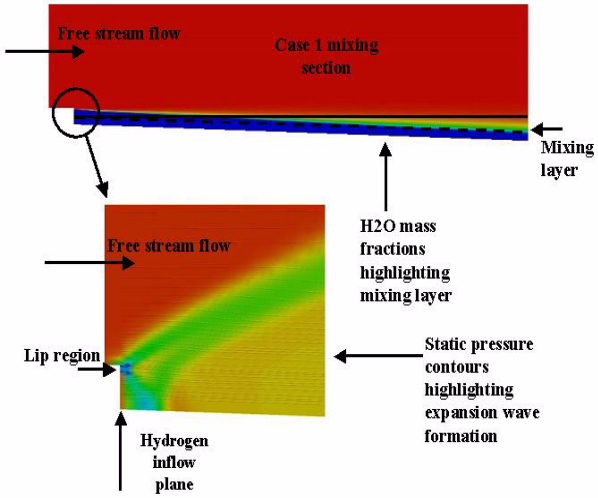

Figure 3: Case 1, zoomed and unzoomed views of mixing section with hydrogen stream on bottom and freestream on top.

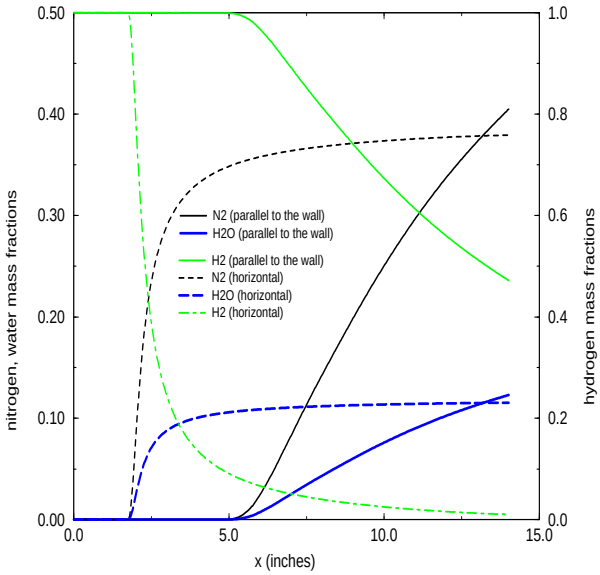

Figure 4: Case 1, axial variation of H_2O, N_2, H_2 mass fractions following the wall (solid lines), and horizontal or true *x*-direction (dashed lines). Both start at the hydrogen entrance 0.0785 inches off the bottom wall.

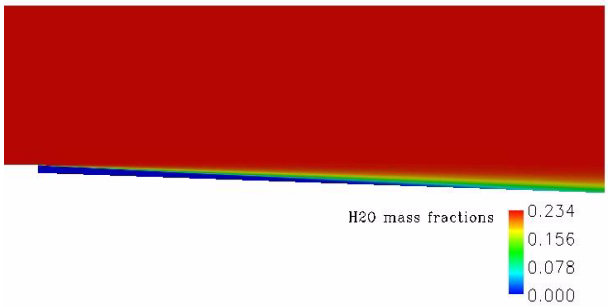

Figure 5: Case 1, H_2O mass fraction contours in the x-y plane.

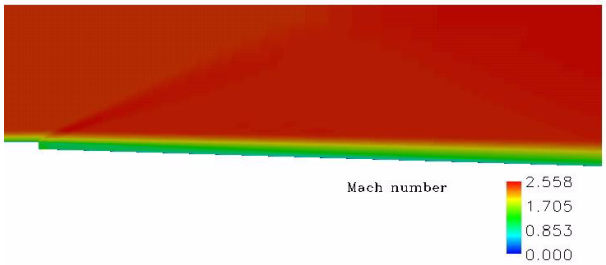

Figure 6: Case 1, Mach number contours in the x-y plane.

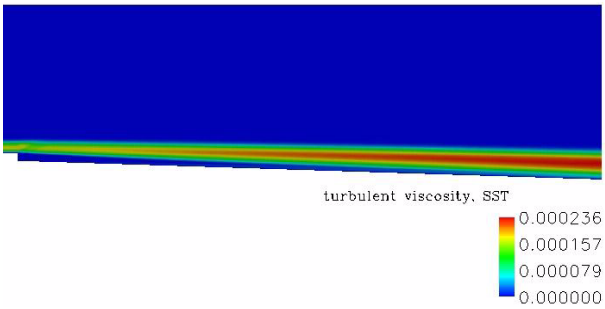

Figure 7: SST turbulent viscosity contours in the x-y plane, indicating the high viscosity being generated in the mixing layer.

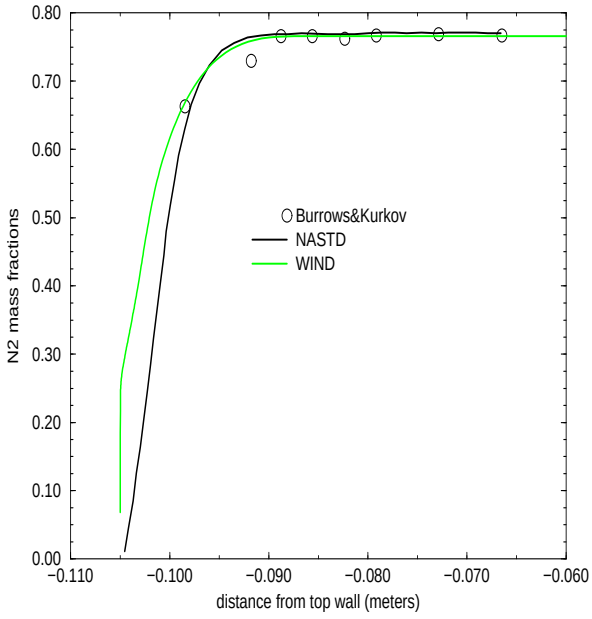

Figure 8: Case 1, nitrogen mass fractions at duct exit.

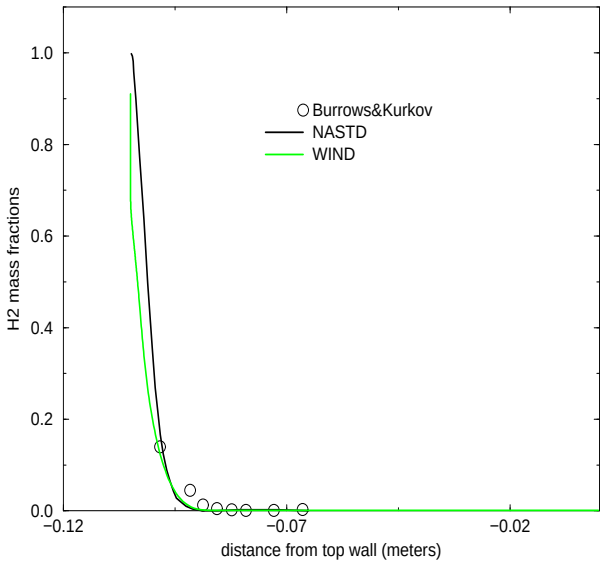

Figure 9: Case 1, hydrogen mass fractions at duct exit.

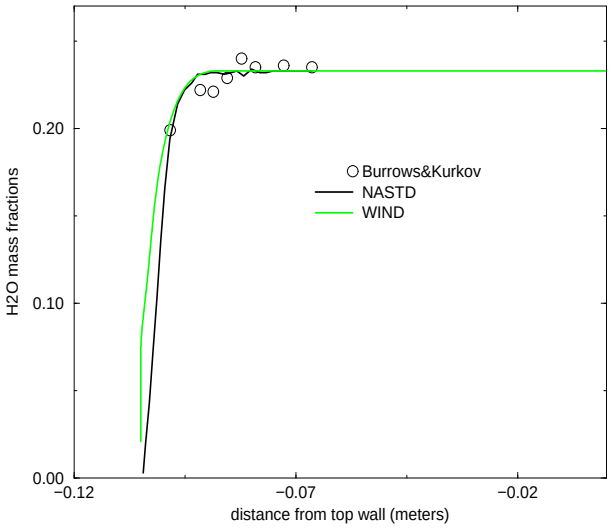

Figure 10: Case 1, water mass fractions at duct exit.

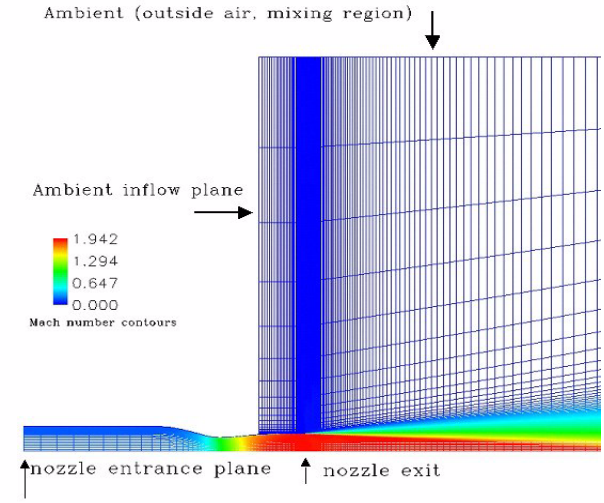

Figure 11: Definition of geometry for Case 2, showing inflow planes and nozzle geometry. The grid structure is colored by Mach number.

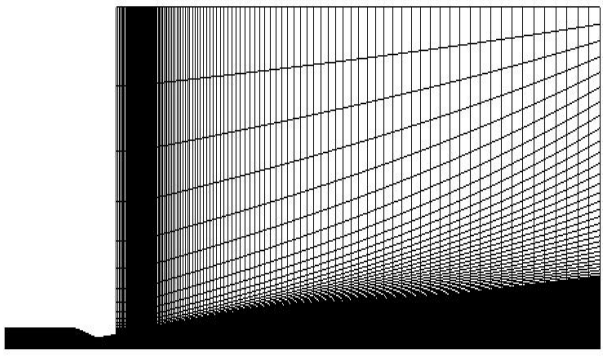

Figure 12: Three-zone grid for Case 2. The mixing section is 121x121 points.

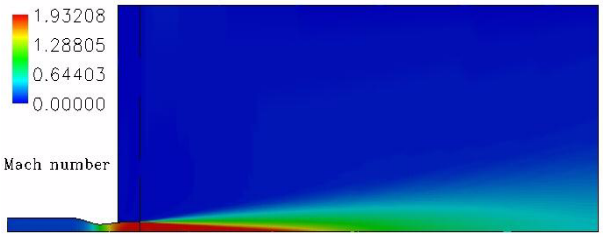

Figure 13: Case 2, Mach number contours for Subcase 2B (frozen).

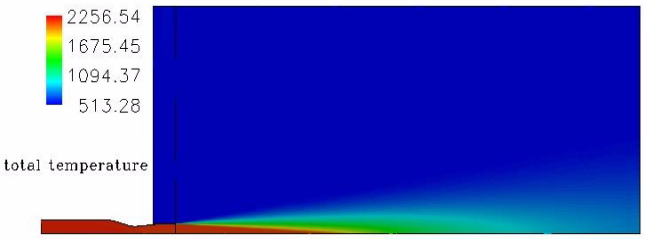

Figure 14: Case 2, total temperature (R) contours for Subcase 2B (frozen).

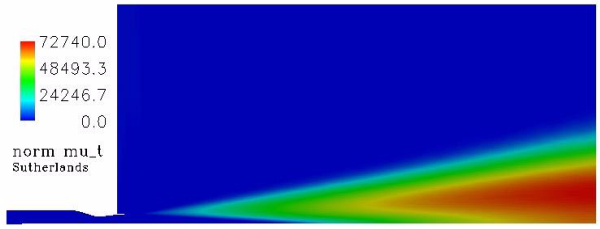

Figure 15: Case 2, normalized turbulent viscosity contours (SST) for Subcase 2B (frozen) using Sutherland's law to compute the laminar viscosity.

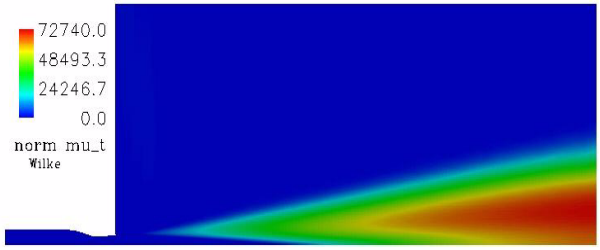

Figure 16: Case 2, normalized turbulent viscosity contours (SST) for Subcase 2B (frozen) using Wilke's law to compute the laminar viscosity.

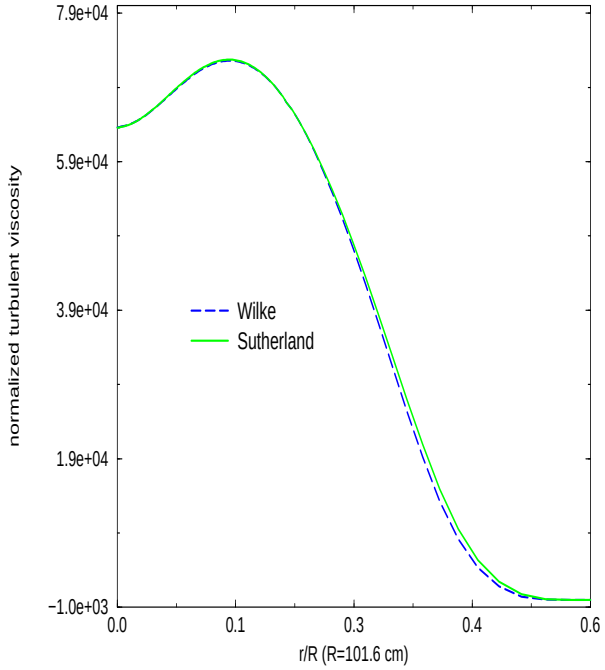

Figure 17: Case 2, normalized turbulent viscosity profiles at the outflow of the computational domain for Subcase 2B (1550F, frozen) comparing the effects of the Wilke and Sutherland viscosity laws.

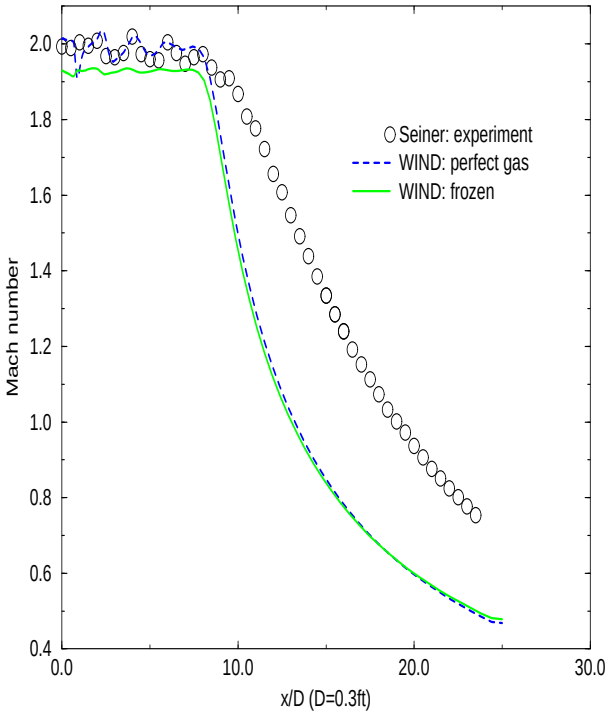

Figure 18: Case 2, Mach number decay along the nozzle centerline for Subcase 2B (1550F).

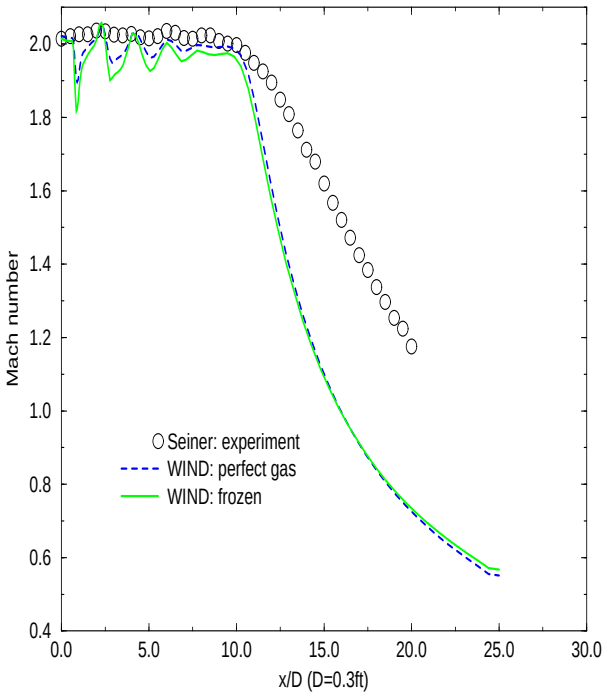

Figure 19: Case 2, Mach number decay along the nozzle centerline for Subcase 2A (104F).

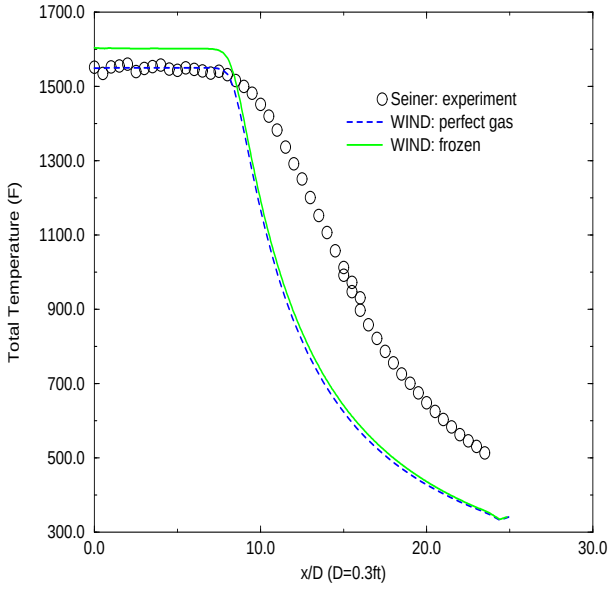

Figure 20: Case 2, total temperature decay along the nozzle centerline for Subcase 2B (1550F).

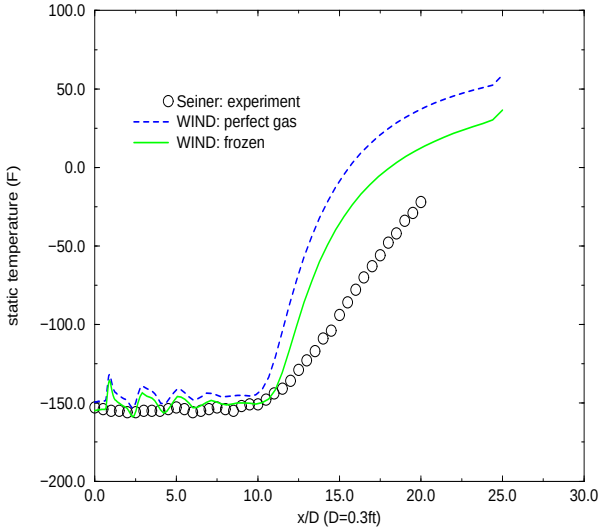

Figure 21: Case 2, static temperature profiles along the nozzle centerline for Subcase 2A (104F).

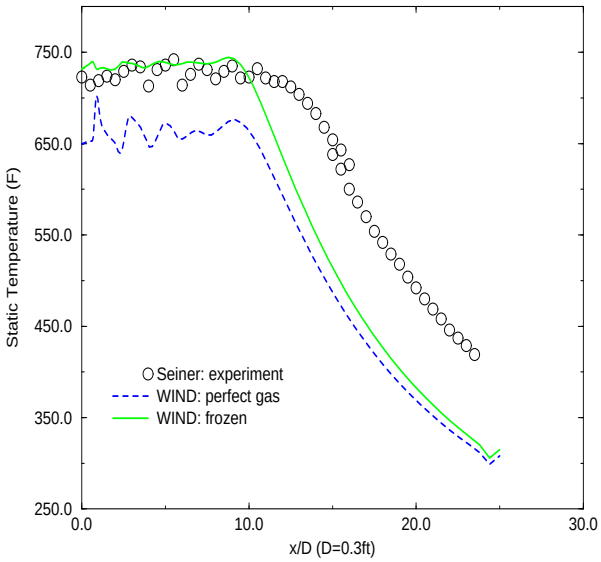

Figure 22: Case 2, static temperature decay along the nozzle centerline for Subcase 2B (1550F).

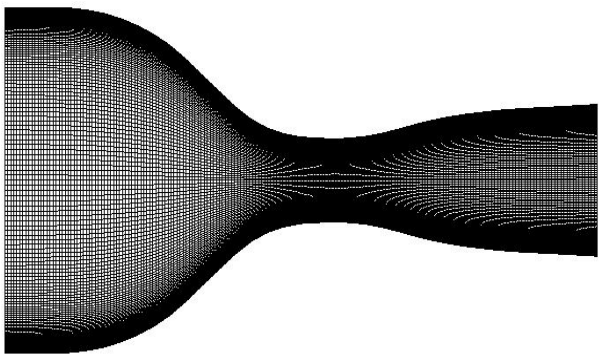

Figure 23: 197x257 grid for Case 3.

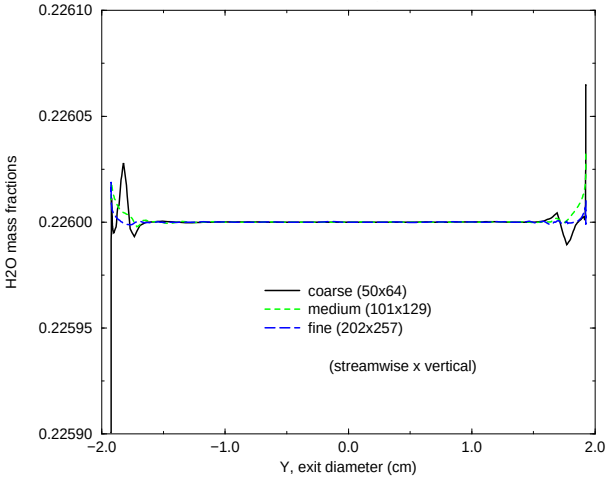

Figure 24: Case 3, H_2O mass fractions at exit plane, showing coarse, medium, and fine grid solution results.

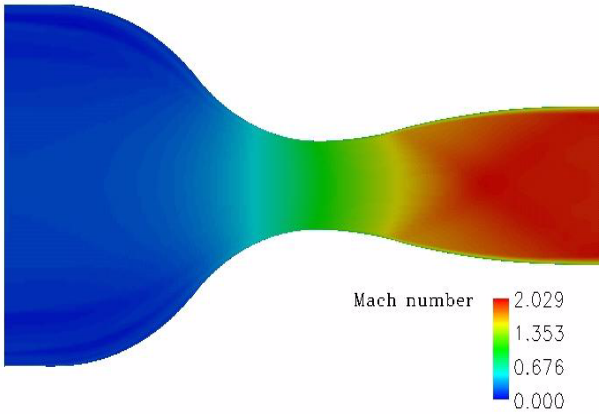

Figure 25: Case 3, Mach number contours in the *x-y* plane for the frozen chemistry case.

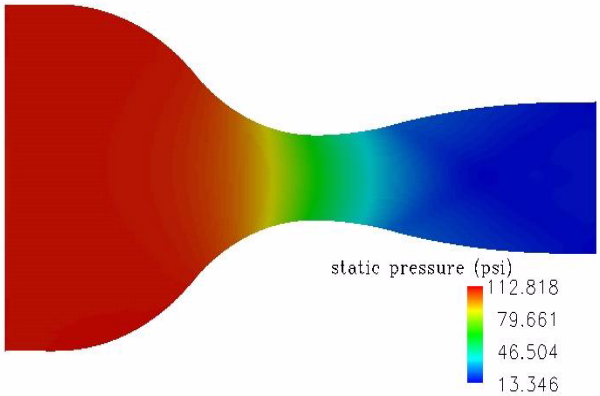

Figure 26: Case 3, static pressure contours in the *x-y* plane for the frozen chemistry case.

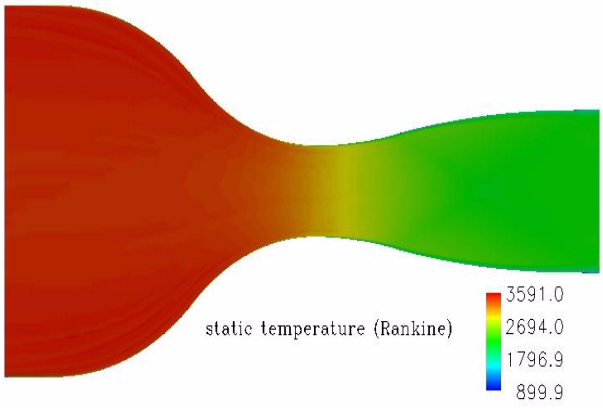

Figure 27: Case 3, static temperature contours in the *x-y* plane for the frozen chemistry case.

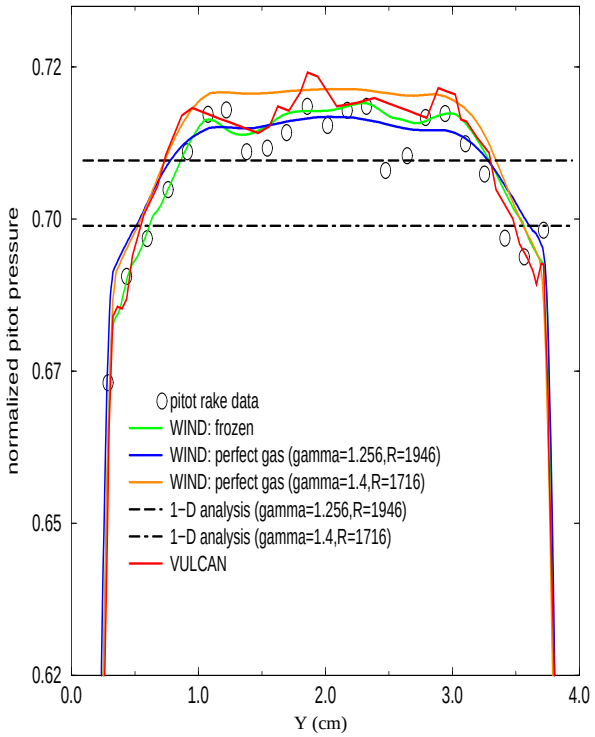

Figure 28: Case 3, plot of pressure at the duct exit comparing WIND frozen and perfect gas models to experiment, numerical results, and 1-D gas analysis. The Pitot pressure is normalized by 7.62 atm (112 psi).

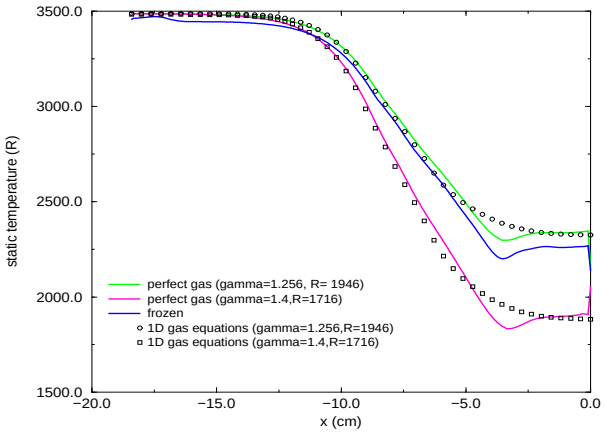

Figure 29: Case 3, plot of static temperature along the duct centerline comparing WIND frozen, and perfect gas models with 1-D analysis.

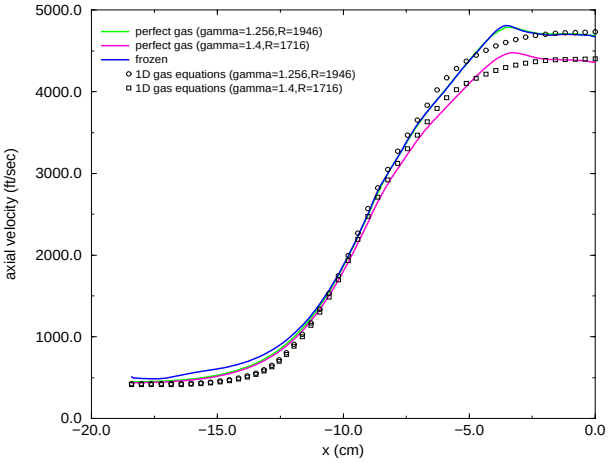

Figure 31: Case 3, plot of the axial velocity along the duct centerline comparing WIND frozen, and perfect gas models with 1-D analysis.

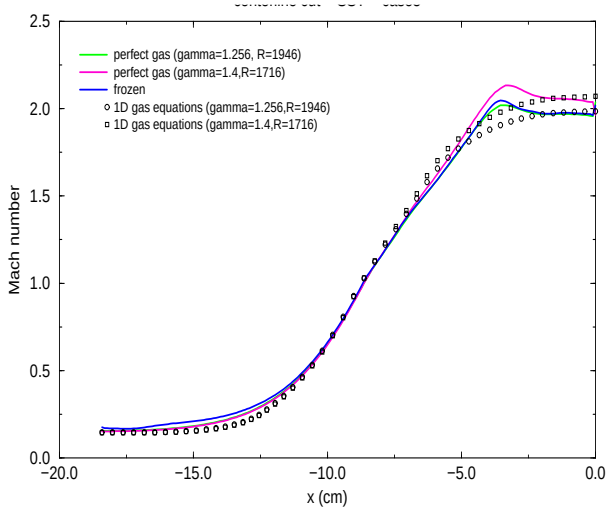

Figure 30: Case 3, plot of Mach number along the duct centerline comparing WIND frozen, and perfect gas models with 1-D analysis.

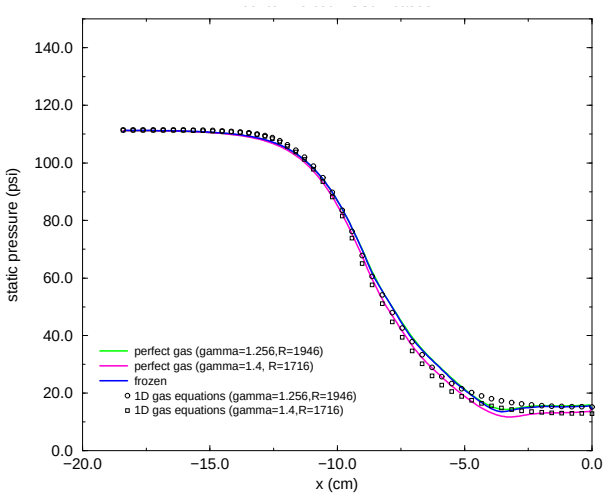

Figure 32: Case 3, plot of the static pressure along the duct centerline comparing WIND frozen, and perfect gas models with 1-D analysis.